J. Mol. Model. **1996**, *2*, 160 – 174

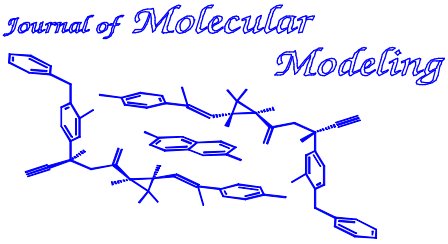

Using Molecular Dynamics to Predict Factors Affecting Binding Strength and Magnetic Relaxivity of MRI Contrast Agents

Yen T. Tan, Richard S. Judson*, and Carl F. Melius

Center for Computational Engineering, MS 9214, Sandia National Laboratories, Livermore, CA 94551-0969, USA (rsjuds@ca.sandia.gov)

John Toner and Gang Wu

Nycomed R&D, Inc., 466 Devon Park Dr., Wayne, PA 19087-8630, USA

Received: 25 March 96 / Accepted: 29 May 1996 / Published: 13 June 1996

Abstract

We demonstrate the use of molecular dynamics and molecular mechanics methods to calculate properties and behavior of metal-chelate complexes that can be used as MRI contrast agents. Static and dynamic properties of several known agents were calculated and compared with experiment. We calculated the static properties such as the *q*-values (number of inner shell waters) and binding distances of chelate atoms to the metal ion for a set of chelates with known X-ray structure. The dynamic flexibility of the chelate arms was also calculated. These computations were extended to a series of exploratory chelate structures in order to estimate their potential as MRI contrast agents. We have also calculated for the first time the NMR relaxivity of an MRI contrast agent using a long (5 nsec) molecular dynamics simulation. Our predictions are promising enough that the method should prove useful for evaluating novel candidate compounds before they are synthesized. One novel static property, the projected area of chelate atoms onto a virtual surface centered on the metal ion (gnomonic projection), was found to give an effective measure of how well the chelate atoms use the free space around the metal ion.

Keywords: Diagnostic imaging, contrast reagents, molecular modeling, chelate, molecular flexibility

Introduction

Magnetic resonance imaging (MRI) has become one of the standard diagnostic tools used by physicians. However, the time-consuming nature of this procedure and the related expense make it important to extract the maximum amount of useful information from each scan. Paramagnetic imaging agents[1] are heavily used today to enhance the contrast in MRI scans in specific ways and hence to increase their information content. Typical agents are comprised of a paramagnetic ion (typically Mn^{+2} or Gd^{+3}) bound by a chelate, which is itself perhaps bound to a protein or other polymer. The unpaired electron spins on the paramagnetic ion create a local magnetic field that couples to the nuclear spin on nearby water protons, which greatly increases their relaxation rate. MRI scans are typically run near saturation, so quicker relaxation enables more power to be absorbed in the regions of the body containing significant concentrations of the agent, which in turn increases the image contrast.

* *To whom correspondence should be addressed*

Successful new MRI contrast agents need to meet at least two design criteria: (1) They have to provide significant contrast enhancement, which translates into a requirement that $1/T_1$ for solutions of the compound be large. (2) They have to be stable with respect to dissociation of the ion-chelate complex. This is due to the high toxicity that is typical of both the free ion and the free chelate. These chelators must bind strongly to the Gd ion even in the presence of other free cations that are normally present in the body. The paramagnetic properties of these agents have been the subject of several recent reviews.[1-5]

In this paper, we demonstrate the use of molecular mechanics and dynamics methods to evaluate chelate structure and function. One factor that is important for the stability of a compound is the dynamic behavior of the chelate arms. What appears from a static structure to be a good binder may in fact be dynamically very mobile. To this end, we give results of several molecular dynamics simulations of chelates in water. These simulations were performed on both known compounds and on several proposed compounds with different binding characteristics. We concentrate on carboxyl groups that can bind in either the bidentate or monodentate conformation to the paramagnetic ion, and examine the structural effect of having two binding oxygen atoms that are equidistant from the ion, vs. a lone binding oxygen atom. An important result is that monodentate carboxyl groups are held more rigidly than are the corresponding bidentate ligands.

Next, we describe a procedure for calculating relaxivities for typical paramagnetic imaging agents and show that reasonably accurate predictions are possible. Relaxivities ($1/T_1$) are a function of the time-dependent positions of water protons relative to the paramagnetic ion.[6] The procedure involves computing long (5 nsec) trajectories of the chelate-metal compound in a water bath and then calculating certain well known correlation functions of the proton-ion vectors. From approximate analytic models,[6,7] it is known that important factors determining $1/T_1$ include the rotational correlation time of the complex, the rate at which waters exchange between the inner and outer solvation spheres, and the number of waters in the inner shell of the ion. This makes it important to accurately model the dynamical interactions of the metal ion, the chelate, and nearby waters. We include electronic effects with an approximate analytic model.

Finally, we look at the static geometric properties of several chelates based on the recognition that there is a limit to the number of chelate groups that can be employed to bind a metal ion. The number of binding sites plus the number of water molecules in the inner solvation sphere of the ion, denoted by q_{tot}, equals the fixed coordination number of the ion, which is between 6 and 10, depending on the ion. For a given value of q_{tot}, and hence a fixed number of coordinating chelate groups, the binding strength is at least partially determined by how the molecule uses the space around the metal ion. The arms connecting the chelating groups need to be flexible enough to allow all of the groups to be optimally placed around the ion at the proper ion-to-chelate atom distance. An effective chelate structure should be capable of maximizing the attraction between the positive ion and negative chelating groups while minimizing the repulsive interactions between different chelating groups. For instance, a chelate with a rigid backbone could leave gaps in the coverage of the surface of the metal ion, decreasing the potential binding energy while simultaneously forcing negatively charged groups to be relatively close together. We demonstrate a method to evaluate the effectiveness of a number of common chelating agents whose 3-dimensional structures are known from X-ray data, and show that commonly used MRI compounds make maximal use of the available surface area of the ion.

Several other groups have used molecular mechanics methods to study metal ion chelate complexes. Hancock and co-workers[8-10] have reported extensive molecular mechanics calculations of ion-chelate systems, concentrating on the concept of steric strain. The strain energy is the sum of all bond length, bond angle, torsional distortions, and van der

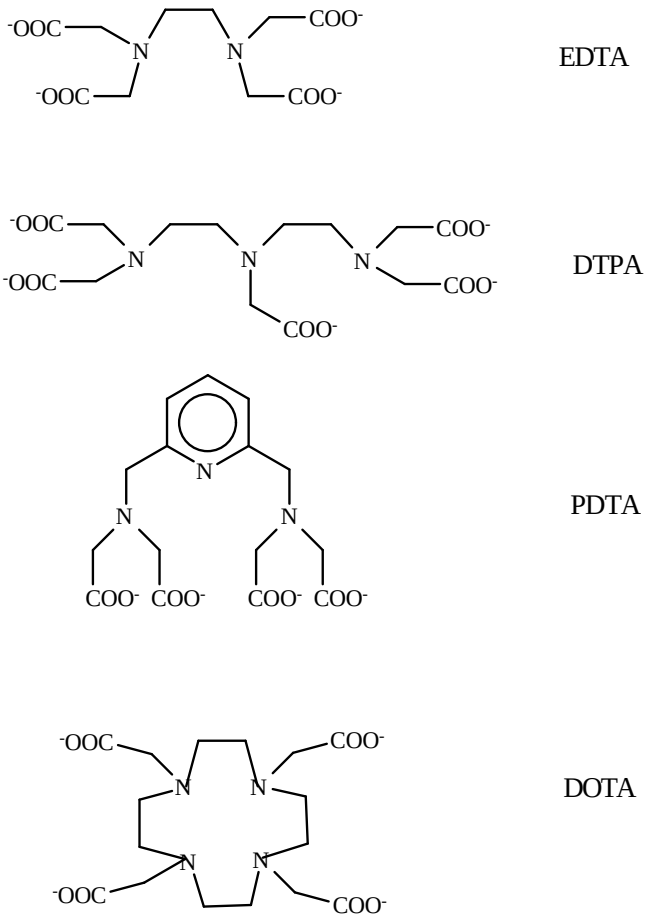

Figure 1. *Chelate structures of MRI contrast agents analyzed in the molecular dynamics simulations. The first panel shows existing compounds. The second panel (following page) shows proposed derivatives of PDTA also examined here.*

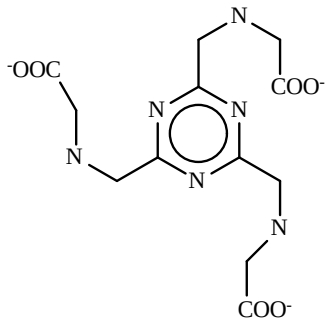

P3A

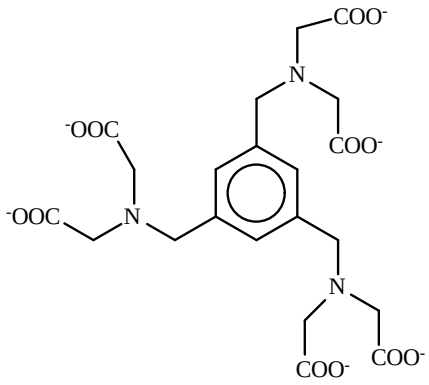

P6A

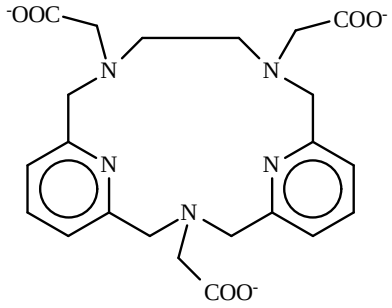

2P3A

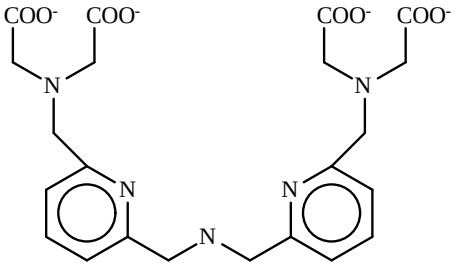

2P4A

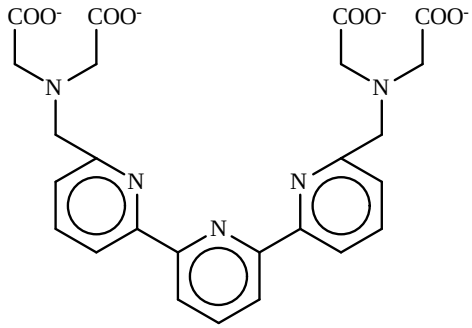

3P4A

Waals interactions in the molecule. Complexes with high strain energy are less likely to form than those with less strain energy. Fossheim, et al.[11,12] performed extensive molecular mechanics and dynamics simulations on lanthanide ion-chelate complexes. Their aim was to study the structure and energetics of free ligands and the corresponding ligand ion complexes, including the important effects of solvation. Among other interesting findings, they report strong correlations between molecular mechanics interaction energies and experimental binding constants. They also investigated the dynamics of complexation, i.e. the process whereby the ligand captures an ion in solution. Kumar and Tweedle[13] report similar calculations on a series of cyclic polyamino complexes. They find a good correlation between ligand strain energy and the energy of reorganization from the proposed final intermediate (one carboxyl group protonated) to the fully

formed, deprotonated ligand-ion complex. Frey and co-workers[14] compare the results of molecular mechanics calculations with luminescence spectroscopic measurements of Eu(III)-ligand complexes. They use molecular mechanics calculations to both determine low energy conformations and to help interpret the spectroscopic results. In particular, they get good agreement for the number of inner shell waters. Another interesting result is that the excitation wavelength for the Eu ion correlates well with the sum of partial atomic charges of the chelating atoms. Hay,[15,16] Rappe, et al.[17] and Badertscher, et al.[18] have developed special purpose molecular mechanics force fields specifically tailored for use with metal-chelate complexes. Hay has published a review of work in this area.[16] With the exception of the work by Fossheim, et al.,[11,12] all of these papers concentrate on static properties of the metal-chelate complexes, while we concentrate on the dynamic properties of these complexes. The calculations we report are also quite different from those in the Fossheim papers.

For the studies in this paper, we have selected a group of chelating agents that contain different numbers of carboxyl and amine binding groups. This group includes two compounds for which much experimental data are available:[5,12,19,20] EDTA **[1]** (ethylene-diamine-tetraacetic acid), and DTPA **[2]** (diethylene-triamine-pentaacetic acid). In addition, calculations were also conducted for DOTA **[3]** (cyclododecane-tetraacetic acid)[21] and a new compound, PDTA **[4]** (pyridine-diamine-tetraacetic acid)[22] and its derivatives. The structures of the chelates used for this study are shown in Figure 1.

X-ray structure data, stability constants and MRI relaxivities are available for DTPA, EDTA, DOTA, and PDTA.[21-27] DTPA has five carboxyl groups and three amine nitrogens while EDTA and PDTA both have four carboxyl groups and two amine nitrogens. DOTA is a cyclic compound with four nitrogens and four carboxyl groups. The thermodynamic stability constants for DTPA and DOTA (Gd(chelate) $\longrightarrow$ Gd + chelate) are considerably higher than that of EDTA, as shown in Table 1. [5,26-28] However, EDTA has a higher *q*-value than DTPA and DOTA and hence a higher MRI relaxivity, $1/T_1$ (see Table 1). Thus EDTA would be more effective as an MRI contrast agent if it were not for the toxic effects arising from its lower stability constant and the resulting release of free Gd ions in the body.

Table 1. *Experimental properties of several Gd chelates*

Compound	log K [a]	*q* [b]	$1/T_1$ (20 Mhz) [c]
Gd^{+3}	NA	9	16.1
$Gd(EDTA)^-$	17.4	3	7.6
$Gd(DTPA)^{2-}$	22.5	1	4.8
$Gd(DOTA)^-$	24.7	1	4.7
$Gd(PDTA)^-$	18.6	2	6.3

[a] Log K is the thermodynamic stability constant for Gd(Chelate) « Gd + Chelate.[1]
[b] q is the number of inner shell waters.
[c] Relaxivity at 20 MHz and 25 C.[1]

Dynamic Behavior of Chelates

In this section, we describe molecular dynamics calculations performed on a series of chelates to characterize their dynamic behavior of the binding groups. In particular, we examine the difference in dynamic behavior between chelates with mono and bidentate carboxyl groups. We calculate mean distances from the Gd ion to chelating atoms, as well as the standard deviation of this distance. The standard deviation provide a measure of the vibrational flexibility of these interactions. As we will show, several of the exploratory compounds assume a bidentate conformation relative to the metal ion, and their carboxyl groups exhibit great mobility.

A. Molecular Mechanics Details

Molecular dynamics calculations were conducted on EDTA **[1]**, DTPA **[2]**, DOTA **[3]**, and PDTA,**[4]** plus its derivatives. Each molecule was solvated using the SPC/E water model of Berendsen.[29] For most molecules, a 12 Å water sphere was used for solvation and the proper water density was maintained by employing a 13.5 Å repulsive spherical shell having a harmonic force constant of 100. The SETTLE algorithm[30] was used to constrain the waters in their equilibrium conformation. A variety of cutoff schemes were tried, but most failed to adequately treat the high electrostatic forces arising from the Gd^{+3}. The method developed by Levitt was selected for use in these computations.[31-33]An atom-based, non-bonded list is used. The original Coulomb (E_q^0) and van der Waals (E_{VDW}^0) terms are replaced by the following:

$$E_q = E_q^0 \times \left(1 - 2(r/r_c) + (r/r_c)^2\right) \tag{1}$$

and

$$E_{VDW}(r) = E_{VDW}^0(r) - E_{VDW}^0(r_c) - \\ -(\partial E_{VDW}^0 / \partial r)(r_c) \times (r - r_c) \tag{2}$$

for $r < r_c$. Both terms are set to zero for $r \geq r_c$, where the value of r_c used is 7.5 Å. Atom pairs are included in the non-bonded list if they are closer than 9.0 Å. The non-bonded list was updated every 10 time steps or 0.01 ps. Berendsen's temperature rescaling method[29] was used with a time constant of 0.1 psec. All runs were performed at 300 K using CCEMD,[34] a general purpose molecular dynamics program based on the MD code of Windemuth and Schulten.[35] We

use the CHARMm force field[36] with QUANTA3.3 [37] parameters for the chelates.

Chelate charges were determined from SCF calculations on chelate fragments. Charges for the solvated species were then calculated by using a boundary element method to match the SCF wavefunction to a continuum solvent.[38] The calculations were performed using a modified version of Gaussian 92.[39] Geometry optimizations of chelate fragments binding to the Ca ion were first performed using the 6-31g* basis set. A self-consistent solvation energy calculation was then performed to determine solvation energies and charges. The 6-31g** basis set was used for these calculations. Charges were averaged to equal -0.65 for carboxylate oxygens, to +0.45 for carboxylate carbons, to -0.50 for backbone nitrogens, and to -0.40 for ring nitrogens. The same charge and atom type were used for both of the two carboxylate oxygens, regardless of their conformation relative to the metal ion. Small adjustments in charges, 0.05 or less, were sometimes made to carbons and hydrogens to assure charge neutrality for the metal-chelate complex. (All input files used for these computations, which include charges, atom types, and force field parameters, can be obtained from the authors upon request.)

We attempted to adjust the van der Waals parameters for the ligand and metal atoms in order to have all ligand-metal distances assume their crystal values. However, these distances also depend on the bond angles and distances within the chelate as it wraps around the metal, and without changing these parameters significantly the metal-ligand distance requirements could not be satisfied. In the end we left all force field parameters at their default values, except for the Gd van der Waals parameters, which were adjusted to give the proper Gd-O distances. The final values are 2.0 • for the van der Waals radius and 0.026 kcal/mol for the well depth. Using these parameters, energy minimization of the chelate molecules resulted in Gd-O distances that were very close to those found in the crystal structures of EDTA and DTPA.[21,23-25] The Gd-N distances are too small. After equilibration (discussed in the next paragraph) we recorded the Gd-O and Gd-N distances from these chelates and compared them with the corresponding crystal structure values. The Gd-O distances for the model and the crystal are (2.40,2.42), (2.40,2.38), and (2.30,2.37) for EDTA, DTPA, and DOTA respectively. The corresponding Gd-N distances are (2.45,2.65), (2.61,2.70), and (2.62,2.68). We should note that other authors achieved better Gd-N distances for these and similar chelates using different force field parameterizations.[11,12,14]

The self-diffusion coefficient for water in the simulations had a value of 2.2×10^{-5} cm^2/sec which compares well with the quoted experimental value of 2.4×10^{-5} cm^2/sec.[29] Prior to the data-gathering runs, the ensembles were equilibrated by annealing to 300 K over an interval of 12 ps with a temperature window of 40 K. Using CCEMD, molecular dynamics runs were conducted for a period of 100 ps to assure adequate statistics for the Gd-ligand non-bonded distances.

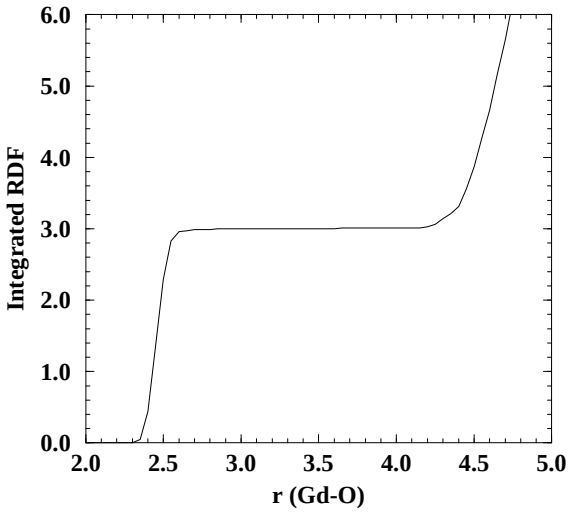

Figure 2. *Integrated radial distribution function for water is plotted as a function of the Gd - water oxygen distance. The inner shell of Gd in Gd-EDTA is shown with three waters (q = 3.0).*

B. Results

From molecular dynamics runs, it is possible to obtain information on the structure of the chelate as well as the distance between specific binding atoms in the chelate and the Gd ion. The MD runs were of 100 psec duration. Inter-atomic distances were collected every 0.1 psec. For the reference compounds, EDTA **[1]** and DTPA **[2]**, as well as DOTA **[3]**, and PDTA **[4]**, the carboxylate groups were all in the monodentate conformation, with one carboxyl oxygen close to the Gd ion and the other displaced away from it. In EDTA, the near oxygen is at an average distance of 2.41 Å while the far oxygen is at 4.32 Å. From an average of the X-ray data, the corresponding distances are 2.40 Å and 4.48 Å respectively.[21,23,24] For DTPA, the average distance values for the near oxygen is 2.37 Å, which is almost identical to the X-ray distance of 2.38 Å. For DOTA, the near oxygen is 2.37 Å from MD simulations and from X-ray data. The average distance of binding nitrogens from the metal ion in EDTA is 2.41 Å vs. 2.65 in the crystal. For DTPA, the corresponding distances are 2.58 and 2.70. For DOTA, the average MD and crystal distances are 2.59 and 2.68 Å. Although the calculated Gd-N distances are too short, we do not believe that a better parameterized model would significantly alter any of our qualitative conclusions.

During the course of an MD run, the radial distribution function of water molecules around the metal ion was monitored. For bare Gd in water, the calculated average Gd - O_{water} distance equals 2.44 Å. The integrated radial distribution func-

Table 2. *Dynamics data on known and proposed MRI contrast agents.*

Compound	Carboxyl [a]	Amide [b]	q [c]	q_{tot} [d]	$\langle d_O \rangle$ [e]	$\langle \sigma_O \rangle$ [f]	$\langle d_N \rangle$ [g]	$\langle \sigma_N \rangle$ [h]
EDTA	4-mono	2/2	3.0	9.0	2.41 / 4.32	0.06 / 0.10	2.41	0.05
DTPA	5-mono	3/3	1.0	9.0	2.37 / 4.34	0.06 / 0.10	2.58	0.09
PDTA	4-mono	3/3	2.0	9.0	2.38 / 4.29	0.05 / 0.11	2.56	0.09
DOTA	4-mono	4/4	1.0	9.0	2.37 / 4.32	0.06 / 0.11	2.59	0.09
P3A	1-mono	1/5	2.9	8.9	2.39 / 4.4	0.06 / 0.11	2.62	0.14
	2-bi				2.44 / 2.7	0.08 / 0.59		
P6A	4-mono	0/3	3.0	9.0	2.42 / 4.0	0.08 / 0.22	4.1-5.3	0.16
	1-bi				2.45 / 2.49	0.07 / 0.08		
2P3A	3-mono	5/5	0.9	9.0	2.37 / 4.3	0.04 / 0.22	2.50	0.07
2P4A	4-mono	5/5	0.0	9.0	2.39 / 4.3	0.06 / 0.10	2.55	0.09
3P4A	4-mono	5/5	0.2	9.2	2.39 / 4.3	0.07 / 0.11	2.58	0.10

[a] Number of mono and bi-dentate carboxyl groups binding to the Gd.
[b] Number of nitrogens binding to the Gd / total number of nitrogens.
[c] Dynamical value of q. This is the time-averaged number of waters in the inner shell.
[d] Total dynamically calculated coordination number of the Gd.
[e] Average distance of the carboxyl oxygens from the Gd (near/far).
[f] Dynamics variation of $d_{Gd\text{-}O}$ (near/far).
[g] Average distance of the nitrogens from the Gd.
[h] Dynamics variation of $d_{Gd\text{-}N}$.

tion for water molecules surrounding Gd-EDTA is shown in Figure 2. From the plateau of the curve, it is observed that there are three water molecules in the first shell that are directly coordinated to Gd^{+3} and hence q=3 (here q denotes the number of first shell waters only) for EDTA. For DTPA, the corresponding q-value obtained from MD runs is q=1. The MD results are summarized in Table 2. As expected, EDTA, with four binding carboxyl oxygens and two nitrogens has a q of 3.0, while DTPA, with five binding oxygens and three nitrogens has a q of 1.0.[19] Non-integer values are sometimes obtained when waters exchange in and out of the inner sphere and spend a small portion of the observed time in the bulk solvent. Results for the other molecules are also given in Table 2. PDTA, with four binding carboxyl oxygens and three nitrogens, has a q of 2.0, while DOTA with four oxygens and four nitrogens has a q of 1.0. MD simulations for the reference molecules all show Gd with a coordination of nine and binding distances that are in good agreement with X-ray data. Note that the most effective MRI contrast agents, DTPA and DOTA, both have a q-value of l and have all of their carboxylate groups in the monodentate conformation.

We ran simulations of several analogues of PDTA **[4]**, some of which were anticipated to show bidentate behavior. These molecules have structures that are similar to the PDTA molecule, but have varying numbers of nitrogens and carboxyl groups attached to the pyridine ring(s) (Figure 1). When the number of binding carboxyl and amide groups drops below six (the number for EDTA), sufficient space becomes available around the metal ion for one or more of the carboxyl groups to assume a bidentate configuration, in which the two oxygen atoms are approximately equi-distant from the Gd ion. As shown in Table 2, the bidentate conformation is observed in the calculated results for P3A **[5]** and P6A **[6]**. (In our nomenclature, the number preceding the "P" indicates the number of pyridine rings in the molecule, is omitted when that number is 1, and the number preceding the "A" indicates the number of acetic acid groups in the molecule.) In the structures where both monodentate and bidentate conformations occur, the Gd-O distance is calculated to be larger for the bidentate carboxyls, 2.44 Å vs. 2.39 Å in P3A **[5]**, and 2.45 Å vs. 2.42 Å in P6A **[6]**. This trend is in agreement with X-ray data (discussed in Section IV) that show a distance of 2.46 Å for a structure having bidentate carboxyl oxygens and 2.38 Å for the average monodentate oxygen-metal distance (for EDTA, DTPA, and DOTA). The resulting small increase in the Gd-O distance could decrease the electrostatic component of the interaction energy. Due to ion-induced polarization effects between the carboxyl oxygens,[38] the electrostatic binding strength of the two oxygens in a bidentate conformation to Gd is predicted to be weaker than that from two monodentate oxygens that are parts of two separate carboxyl groups. Thus the monodentate conformation should be stronger in terms of binding per carboxyl oxygen, even in the absence of increased Gd-O distance for the bidentate conformation.

The MD results for the average Gd-O and Gd-N distance and the accompanying dynamic variation values, σ_o, give an indication of the extent of motion of the chelate atom relative to the ion, as shown in Table 2. A large value of s_o implies large flexibility, and conversely, a small σ_o implies little flexibility. When the carboxyl group is in the monodentate

conformation, the binding Gd-O distance varies between 2.37 and 2.42 Å with a σ_o of about 0.06 Å. The far oxygen distance is about 4.3 Å and its σ_o is significantly larger (0.11 - 0.22) showing that the outer carboxyl moves more freely than the inner one. In the monodentate conformation, the carboxyl group essentially pivots about the near oxygen. In the bidentate conformation, the size of the σ_o value depends on whether the two oxygen atoms are equidistant from the metal ion or if one is closer than the other (P6A **[6]** vs. P3A **[5]**). When the bidentate conformation is imperfect, as in P3A, the oxygen slightly further from the metal ion will have a larger σ_o value and is hence more flexible. This gives an indication of the fluidity of motion found with bidentate oxygens.

Of the exploratory molecules examined, all five structures were able to achieve a total coordination number of 9. For the molecules containing multiple pyridine rings (2P3A **[7]**, 2P4A **[8]**, and 3P4A **[9]**), all of their carboxyl groups take on a monodentate conformation. These molecules have more binding nitrogens than carboxylate groups, with 5 binding nitrogens and 3 to 4 monodentate oxygens. This differs from the reference chelates that have either more binding carboxyl oxygens than binding nitrogens (EDTA, DTPA, PDTA) or an equal number (DOTA). DTPA, for instance, has three nitrogens and five monodentate oxygens. Of the exploratory structures, 2P3A **[7]** has a *q*-value close to one, a characteristic of both DTPA and DOTA, while 2P4A **[8]** and 3P4A **[9]** have a *q*-value close to zero. If *q*=1 is essential for sufficient contrast enhancement of MRI images, 2P3A **[7]** should be a good candidate. Its usefulness as a potential MRI contrast agent would then depend on whether nitrogens are as effective as carboxyl oxygens in binding to the Gd. Two exploratory molecules, P3A **[5]** and P6A **[6]**, contained carboxyl groups in the bidentate conformation and a *q* of 3. When the chelate binding atoms are taken into consideration, a q_{tot} of 9 is attained. These simulations have thus shown that a Gd coordination number of 9 is obtained, both for the reference compounds and the exploratory structures.

Predicting Relaxivity

The relaxivity of a paramagnetic ion complex arises from the interactions between rotational and spin degrees of freedom. In this section, we describe a model of relaxivity that combines a first principles description of the rotational contribution to the relaxation which can be described classically, coupled with a phenomenological description of the purely quantum mechanical electron spin resonance contribution.

A. Theory

The theory of relaxation of protons in the presence of a paramagnetic ion is well understood and is treated in depth in a number of texts.[6,7,40] The basic mechanism for relaxation is that as protons move in the vicinity of a paramagnetic ion, they feel a time-varying magnetic field that helps couple the proton magnetization to the thermal bath. The most important coupling mechanisms between the proton spin and the paramagnetic electron spin are dipole-dipole and contact coupling. The contact term arises when the proton penetrates the outer electron shell of the ion. In this paper, we only treat *S* state ions such as Gd^{+3} and Mn^{+2}, for which the contact term can be neglected. The relaxation rate for dipole-dipole coupling, $1/T_1$ equals

$$1/T_1 = \gamma_I^2 \gamma_S^2 \hbar^2 S(S+1)\left(\frac{1}{12} J^{(0)}(\omega_I - \omega_S) + \right. \\ \left. + \frac{3}{2} J^{(1)}(\omega_I) + \frac{3}{4} J^{(2)}(\omega_I + \omega_S)\right) \quad (3)$$

where I=1/2 is the proton spin, S is the electronic spin of the paramagnetic ion, γ_I and γ_S are the gyromagnetic ratios ω_I and ω_S are the Larmour frequencies for the proton and electron spins, respectively. The spectral densities $J^{(0)}$, $J^{(1)}$ and $J^{(2)}$ are Fourier transforms of certain time correlation functions:

$$J^{(i)}(\omega) = \int_{-\infty}^{\infty} dt \; e^{-i\omega t} \; g^{(i)}(t) \quad (4)$$

The time correlation functions are:

$$g^{(i)}(t) = \left\langle \overline{f^{(i)}(t_0) \; f^{(i)}(t + t_0)} \right\rangle \quad (5)$$

where the brackets indicate an ensemble average over all water protons and the bar an average over time origins t_0. The functions *f* are given by:

$$f^{(0)}(t) = \left(1 - 3\cos^2\theta\right)/r^3$$

$$f^{(1)}(t) = \sin\theta \; \cos\theta \; e^{-i\varphi} / r^3 \quad (6)$$

$$f^{(2)}(t) = \sin^2\theta \; e^{-2i\varphi} / r^3$$

whose angular parts are simply unnormalized spherical harmonics, $Y_{2m}(\theta, \varphi)$. The paramagnetic ion is placed at the origin of the laboratory coordinate system; the coordinates (r, θ, φ) give the position of a particular proton relative to the ion. The angular and $1/r^3$ factors arise from the radial part of the dipole-dipole Hamiltonian. Already we can see that the rate of relaxation will be a sensitive function of the dynamics of water protons moving in the vicinity of the ion because of terms of the order of $1/r(t)^6$.

Approximate analytic models of the relaxivity can be derived starting from the assumption that each of the correlation functions $g^{(i)}$ will decay exponentially:

$$g^{(i)}(t) = g_0^{(i)} \exp[-t / \tau^{(i)}] \tag{7}$$

One can then perform the Fourier transforms to arrive at the expression

$$1/T_1 = \gamma_I^2 \gamma_S^2 \hbar^2 S(S+1)\left(\frac{1}{12} \frac{g_0^{(0)} \tau^{(0)}}{1+(\omega_I - \omega_S)^2 \tau^{(0)^2}} + \right.$$
$$\left. + \frac{3}{2} \frac{g_0^{(1)} \tau^{(1)}}{1+\omega_I{}^2 \tau^{(1)^2}} + \frac{3}{4} \frac{g_0^{(2)} \tau^{(2)}}{1+(\omega_I + \omega_S)^2 \tau^{(2)^2}} \right) \tag{8}$$

This can be further simplified by recognizing that the electron Larmour frequency, ω_S, is give by $\omega_S=(\gamma_S/\gamma_I)\times\omega_I$ where (γ_S/γ_I) is 658. Therefore in Eq. 8, $(\omega_S \pm \omega_I)^2 \approx \omega_S{}^2$. Using this relationship together with the approximations, $\tau^{(0)}=\tau^{(1)}=\tau^{(2)}\equiv\tau_c$, and $\omega_I\tau_c<<1$, we arrive at:

$$1/T_1 = \gamma_I^2 \gamma_S^2 \hbar^2 S(S+1) \cdot$$
$$\cdot \left(\left[g_0^{(0)} \Big/ 12 + 3g_0^{(2)} \Big/ 4 \right] \frac{\tau_c}{1+\omega_S{}^2 \tau_c^2} + \left[3g_0^{(1)} \Big/ 2 \right] \tau_c \right) \tag{9}$$

For the special case of a bare ion in water, assuming that on average protons are uniformly distributed about the ion, we can calculate the ratios $g_0^{(0)} : g_0^{(1)} : g_0^{(2)}$ that are 6:1:4. These arise from calculating the integrals

$$r^3 \int_0^{\pi} d\theta \, \sin\theta \left| f^{(i)}(r,\theta,\varphi) \right|^2 \tag{10}$$

This leads to the final approximation:

$$1/T_1 = \gamma_I^2 \gamma_S^2 \hbar^2 S(S+1) g_0 \left(\frac{7}{2} \frac{\tau_c}{1+\omega_S{}^2 \tau_c^2} + \frac{3}{2} \tau_c \right) \tag{11}$$

where g_0 is a constant. So for the bare paramagnetic ion in water, we expect to see a plateau at low frequency which drops off to a second plateau at $\omega \approx 1/\tau_c$. The ratio of the heights of the two plateaus should be 10/3. A further approximation can be included to model the relaxivity due to chelated ions by adding, to Eqs. 9 or 11, a factor which is the fraction of coordination sites open to waters. This accounts for the reduced access of protons to the inner solvation sphere of the ion, where a large portion of the relaxation occurs. This factor is denoted by q/q_0, where q_0 is 9 in the case of Gd^{+3}. Scaling by this factor is not entirely accurate because outer shell waters also account for a small but significant amount of relaxivity. For a q=1 compound, such as DTPA, the outer shell relaxivity accounts for about half of the total.

So far, we have only treated the relaxation of the proton spins and have neglected the simultaneous electron spin relaxation (e.s.r.) of the paramagnetic ion. A first principles treatment of this e.s.r process is difficult, although it has been carried out for several special cases using a variety of approximations for the perturbations due to the motion of nearby nuclear spins.[6,7,40-43] Here we include the effect in an approximate way using the Solomon-Bloembergen-Morgen (SBM) theory.[44,45] Our starting point is Eq. 7 where SBM theory prescribes that the correlation time $\tau^{(i)}$ consists of three components,

$$\frac{1}{\tau^{(i)}} = \frac{1}{\tau_R^{(i)}} + \frac{1}{\tau_M} + \frac{1}{T_e^{(i)}(\omega_S)} \tag{12}$$

where $\tau_R^{(i)}$ is a rotational correlation time, τ_M is the mean lifetime of water protons in the inner shell of the paramagnetic ion, and $T_e^{(i)}$ is the e.s.r correlation time. In SBM theory, the first two correlation times account in a phenomenological manner for the detailed dynamics we directly calculate. The relaxation behavior associated with those terms is built into our numerically calculated correlation functions, $g^{(i)}(t)$. The additional additive term in Eq. (12) can be approximately included into $g^{(i)}(t)$ by multiplying by an exponential term. The correlation function including the e.s.r component is given by[40]

$$\bar{g}^{(i)}(t) = g^{(i)}(t) \exp[-t / T_e^{(i)}(\omega_S)] \tag{13}$$

The functions $\bar{g}^{(i)}(t)$ are then substituted into Eq. 4 to calculate the complete spectral densities. An important property of $T_e^{(i)}$ is its frequency dependence which is given by

$$\frac{1}{T_e^{(i)}} = \frac{1}{5\,\tau_{SO}} \left(\frac{1}{1+\omega_s^2 \tau_v^2} + \frac{4}{1+4\omega_s^2 \tau_v^2} \right) \tag{14}$$

for i=1 and

$$\frac{1}{T_e^{(i)}} = \frac{1}{5\,\tau_{SO}} \left(1.5 + \frac{2.5}{1+\omega_s^2 \tau_v^2} + \frac{1}{1+4\omega_s^2 \tau_v^2} \right) \tag{15}$$

for i=0 and 2. The parameters τ_{SO} and τ_v can be determined experimentally by fitting relaxivities to the full SBM equations.[46] Here, we make the approximation that these parameters will change little from one chelate to the next and use values determined for aqueous Gd^{+3} as a universal set. In

point of fact, the addition of this electronic effect makes minor changes in the predicted relaxivities for small, freely rotating chelates. The values used are τ_{SO}=132 psec and τ_v=16 psec.[46] These values were determined for 25 C. Correcting the values of the parameters for the presence of the chelate will change our numerically determined relaxivities slightly, but will not affect any of our qualitative conclusions.

Before giving the numerical results, we will summarize the computational procedure. A long (5 nsec) molecular dynamics run is performed. From the saved coordinates, the values of $f^{(i)}(t)$ (Eq. 6) are calculated and used in Eq. 5 to give the raw correlation functions $g^{(i)}(t)$. The spectral densities, $J^{(i)}(\omega)$, are computed (Eq. 4) using the modified correlation functions, $\bar{g}^{(i)}(t)$, (Eq. 13). Finally, the values of the relaxivities are calculated from Eq. 3. For our calculations, none of the approximations discussed in Eqs. 7-11 are used.

B. Results

In this section, we present relaxivity results for Gd-EDTA and compare these with experimental data. The molecular dynamics parameters are the same as described in the previous section except that a periodic box of 20 Å on a side was used that contained 249 water molecules**.** The simulation was run for 5 nsec, with the trajectory being saved every 0.1 psec. The calculations reported here took about 600 hrs on an SGI R8000 Power Challenge. During an initial run, one of the three inner shell waters was found to move in and out of the inner shell, with a mean lifetime of about 500 psec. This produced an effective *q* value of 2.5 and yielded a relaxivity that was too small by a factor of about 2.5/3. Consequently, a second run was performed in which 3 waters were constrained to remain in the inner shell, by adding a weak restraining bond between the water oxygens and the Gd ion of length 2.4 Å. The subsequent results were obtained from the constrained run.

In Figure 3 we show the correlation functions $g^{(i)}(t)$ for *i*=0, 1 and 2. In each case, there is an initial short time decay followed by a long time tail. The calculated correlation times, $g^{(i)}(t)$, are each approximately 25 psec. This value is found by fitting the initial decay to an exponential. A direct comparison with experiment is difficult because the experimental correlation times, which are derived from a multi-parameter fit to the dispersion data, include the electronic contribution whereas ours do not, i.e. the calculation measures the initial decay of $g^{(i)}(t)$ (Eq. 5) and not of $\bar{g}^{(i)}(t)$ (Eq. 13). Note that inclusion of the electronic component would decrease our computed correlation times. At t=0, the ratio $g_0^{(0)} : g_0^{(1)} : g_0^{(2)}$ is 5.8:1:4.1 which is close to the ratio 6:1:4 given by the infinite time average for a freely rotating complex (See Eq. 9).

Figure 4 shows the $1/T_1$ dispersion curve along with the experimental values.[3] Before calculating the Fourier transforms in Eq. 4, the correlation times were multiplied by a function that went smoothly to zero at *t*=1.5 nsec. The experimental relaxivity values are indicated by crosses. The calculated total dispersion is given by the solid line while the calculated inner sphere dispersion is shown by a dot-dashed line. Inner shell contributions are calculated by including only contributions from the three bound waters. At the low frequency end, the ratio of computed values to ex-

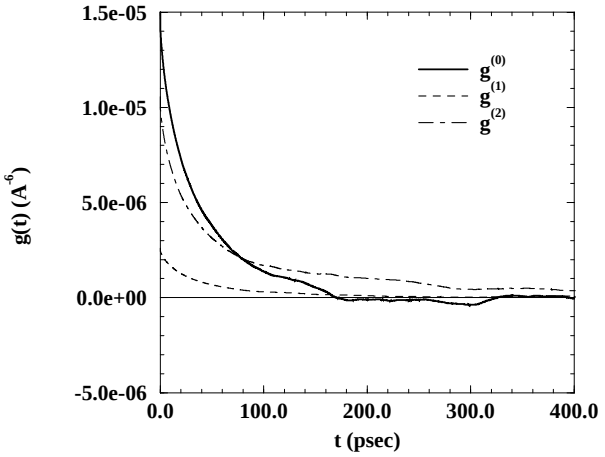

Figure 3. *Time correlation functions* $g^{(i)}(t)$ *for* i=*0 (solid curve),* i=*1 (dash-dot curve) and* i=*2 (dashed curve). The ratios at* t=*0 are 5.8:1.0:4.1. The correlation functions were smoothly damped to zero at* t=*1.5 nsec before calculating the spectra.*

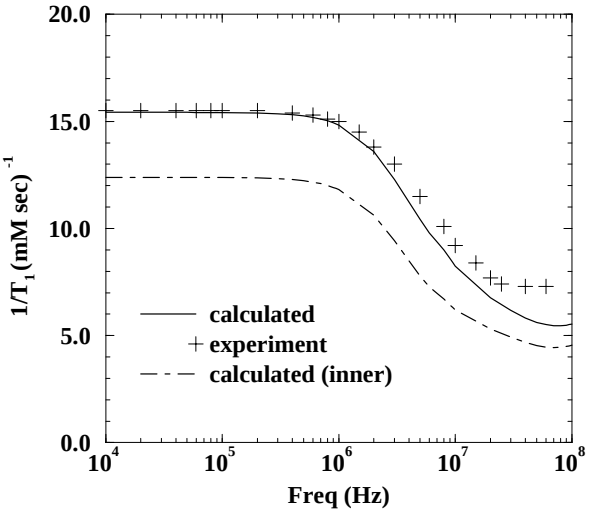

Figure 4. *Comparison between experimental and calculated values of* $1/T_1$. *Experimental data points are indicated by crosses.[3] The calculated values are given by the solid line. The calculated inner-shell relaxivity is given by the dot-dashed line.*

perimental values is 0.99. At the high frequency end (20 MHz) the ratio (calculated/experiment) is 0.75. For the computed results, the ratio of the height of the low frequency plateau to that at high frequency is 10/3.5, in contrast to the ratio of 10/3 predicted from Eq. 11. The experimental ratio is 10/4.8. Recall that Eq. 11 is derived for the case of a bare ion in water. Nonetheless, our predicted high frequency plateau is low, which indicates that the contribution from $g^{(1)}(t)$ is too small relative to the other components. The 3 inner shell contributions account for about 80% of the relaxivity at both low and high frequencies. Therefore, the entire outer shell contribution is $\approx$0.75 of that from one inner shell water, for EDTA.

Another theoretical prediction is that the correlation functions arising from inner and outer sphere process should behave differently.[7] In particular, the inner sphere correlation functions should decay as a single exponential while the outer sphere contributions should die off as a sum of exponentials with increasing correlation times arising from increasingly distant waters. However, as the distances and correlation times increase, these terms will contribute less due to the $1/r^3$ factor in Eq. 6. Our numerical results for the inner and outer shell contributions to $g^{(0)}(t)$ are shown in Figure 5. The results for the other two components of *g* are identical. The outer shell contribution dies off very quickly with a correlation time of about 22 psec. There is no long time tail as for the inner shell contribution. Physically, this makes sense because the outer shell waters are randomized quickly. In the bulk, for instance, the mean time for a pair of waters to exchange position is only about 10 psec.

In conclusion, the agreement between theory and experiment is quite good given that no adjustable parameters were used in the calculations. The calculated low frequency plateau almost exactly reproduces the experimental data, which indicates that the long time average structure of the complex is correctly modeled. The high frequency plateau yields information concerning fluctuations about the average structure, which we have modeled somewhat less accurately. The calculated value is somewhat lower than the experimental result at 20 MHz. A variety of approximations have been made in these calculations that could influence the numerical accuracy of the final results. These include using the experimental values for the electronic relaxation parameters of a bare Gd ion. The force field used will obviously affect the rotational correlation times. This will likely be sensitive to the water model used (charges, internal flexibility, etc.). Small differences in the Gd-O distance can have large effects on the relaxivity values, e.g. an 0.05 Å shift will change the values by >10%. Finally, the long time tails of the correlation functions are not fully converged, i.e. we still see some oscillatory behavior even with 5 nsec of statistics. We performed some approximate calculations using a random walker on a sphere that indicate that full convergence may need on the order of $1000 \times \tau_c$, or about 25 nsec. Future work will aim to understand the importance of each of these postulated sources of error and thereby to increase the quantitative accuracy of the calculations.

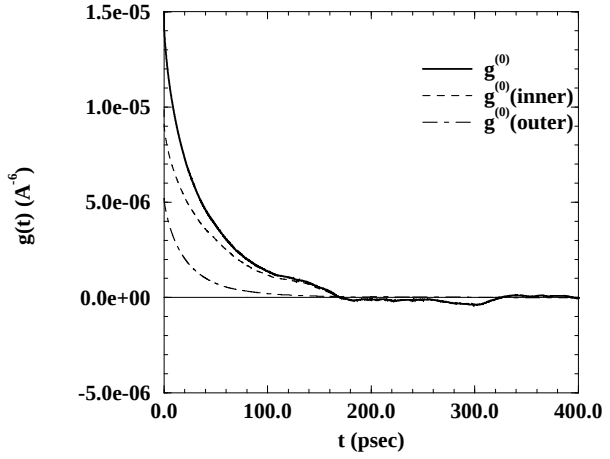

Figure 5. *Total correlation function and inner and outer shell contributions for* $g^{(0)}(t)$. *Note that the outer shell contribution dies off much more quickly than the inner shell component. Comparisons for the other two components of* g *show this same behavior.*

Static Structures - Gnomonic Projections

In this section, we turn to the description of a static method for determining the efficacy with which different chelate binding groups use the space around a metal ion. Gd^{+3}, used as the model paramagnetic ion in this work, has a nominal coordination number of 9, e.g. 9 water molecules will cluster around the unchelated ion with their oxygens pointing towards it. Ions of the lanthanide series have coordination numbers varying from 8 to 10. Smaller ions of the lanthanide series, such as Er (ionic radius of 0.97 Å) have a typical coordination number of 8, while larger ions, such as Ce and La (ionic radii of 1.14 and 1.16 Å) have a typical coordination number of 10.[47,48] In the presence of a chelate such as EDTA, this difference will manifest itself in terms of differing numbers of first shell water molecules around the lanthanide ion, which may vary from 2 to 3. For instance, a coordination of 8 is found for Er(EDTA) which has two first shell water molecules. A coordination of 10 is achieved in crystalline Ce(EDTA) and La(EDTA) with the replacement of a water molecule by a bidentate carboxylate group which can be shared with an adjoining lanthanide ion. The Gd ion with an ionic radius of 1.00 Å is in the group of lanthanide ions having a coordination number of around 9.

A good chelate will be sufficiently flexible to allow its chelating groups to wrap around the metal ion and fill a number of coordination sites in a low energy conformation. An inflexible chelate on the other hand may be unable to relax into a low energy conformation. Two manifestations of

Table 3. *X-ray data on effective areas and binding distances of chelates.*

Chelate	A_{fract} [a]	d_{On}/d_{Of} [b]	d_N [c]	CSD designation
Gd[biacetate]	0.670	2.44 / 2.49	2.62	VEDSEC
Dy[DTPA-Amide]$(H_2O)_1$	0.644	2.34/4.40	2.66	VOSBOU
Gd[DTPA-Amide]$(H_2O)_1$	0.634	2.37 / 4.45	2.70	VETDON
Gd[DOTA]$(H_2O)_1$	0.637	2.36 / 4.43	2.68	KUKGOM
Gd[EDTA]$(H_2O)_3$	0.629	2.40 / 4.48	2.65	BIFZEV
$Gd(H_2O)_9$ [d]	0.626	2.42	NA	
Gd[Pyridine-$(CO_2^-, CO_2H)](H_20)_3$	0.630	2.42 / 4.52	2.55	JOZGUA
Gd[CO_2^--CH_2O-CH_2-CO_2^-]	0.625	2.41 / 4.48	NA	NAOAGD
$(H2O)_3(CF_3CO_2)$Đ	0.571/0.604	2.39	NA	SERYOD
GdĐ$(CF_3CO_2)_4$ĐGd	0.571/0.604	2.39	NA	SERYOD
Đ$(CF_3CO_2)(H2O)_3$	0.571/0.604	2.39	NA	SERYOD

[a] A_{fract} *is the fractional surface area taken up by the ligands, defined in Eq. 2.*

[b] These are Gd distances to the near and far bidentate oxygens in the crystal structure.

[c] These are Gd distances to the backbone nitrogens in the crystal structure.

[d] This is an average of 2 structures

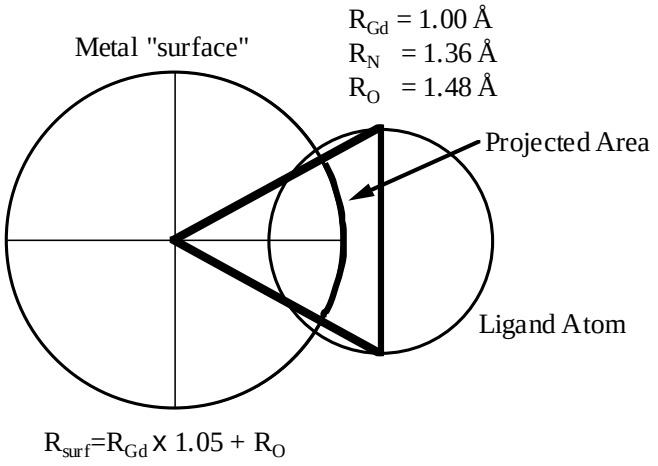

Figure 6. *Diagram showing the construction of a gnomonic projection in cross section. A large sphere is first constructed, centered on the Gd ion, and given a radius* $R_{sph} = 1.05 \times R_{Gd} + R_O$. *Next, a second sphere is centered on each ligand atom. These spheres have the appropriate van der Waals radii for the ligand atoms. For each ligand atom, a cone is drawn with its apex at the center of the metal atom and with its centerline along the line connecting the centers of the Gd and ligand atoms. The cone intersects the ligand atom sphere at a plane containing the center of the ligand atom. The gnomonic projection is then the area of the surface of the metal sphere enclosed by the cone.*

this are that some chelate arms may be forced away from the ion, or chelate arms may be forced to be too close to each other. Each of these will decrease the binding energy, even for a constant value of q_{tot}. Therefore, the effective use of the space surrounding the Gd ion is an important aspect of strong chelate binding. Hancock[8-10] has previously discussed the relationship between chelate flexibility and packing. Another way to analyze this issue is to examine the areas occupied by the chelate oxygen and nitrogen atoms. Here we display and measure these areas using what are termed gnomonic projections. This method involves the projection of the cross-sectional area of a chelate atom onto the surface of a virtual unit sphere whose center is located at the center of the metal ion. We take the radius to be the sum of the ionic radius for Gd and O or N (Figure 6). The ionic radii used here [oxygen (1.36 Å), nitrogen (1.48 Å), Gd (1.00 Å)] were obtained from the comprehensive work of Marcus.[47,48] The radius of the virtual sphere, R_{sph}, is normalized to the nominal Gd - O distance:

$$R_{sph} = 1.05 \times R_{Gd} + R_O \qquad (16)$$

where $R_O = 1.36$ Å is the radius of an oxygen ligand atom. A normalization factor of 1.05 was used to make the radius of the virtual sphere equal to the average Gd - O distance of 2.40 Å, obtained from the X-ray structure of EDTA.[13-15] Through the use of gnomonic projections, a fractional surface area is obtained. We calculate the area of each first shell atom when projected onto the surface of the virtual sphere, and then divide by the total surface area of the sphere. This factor is further normalized by dividing by the fractional area covered by a hexagonal array of spheres on a plane. Therefore, a value of 1.0 for the fractional projected surface (denoted A_{fract}) is the maximum possible. The final result for the fractional projected surface area is:

$$A_{fract} = \frac{\sqrt{3}}{\pi}\left(1 - \frac{D}{\sqrt{D^2 + R_L^2}}\right) \quad (17)$$

where D is the distance from the metal ion to the ligand atom and where R_L is the radius of the ligand atom whose overlap area is being calculated. Our numerical results take into account the case where the projections from different ligand atoms overlap, to make sure that those areas are not double counted. Note that A_{fract} decreases with increasing ligand-metal distance, *D*. Figure 6 shows the construction of the gnomonic projection in cross-section.

From the gnomonic projections, the total projected area on the virtual surface is obtained for the chelate oxygens and nitrogens, as well as for the oxygen atoms from first shell water molecules. The Cambridge Structural Database (CSD) was searched for structures containing a paramagnetic ion and molecules containing oxygen and carbon atoms. The search resulted in a database containing 870 crystal structures. From these structures, those containing Mn, Zn, or multiple ions were discarded. Gnomonic projections were obtained for each compound in the remaining group of 98 crystal structures. In Table 3 we give the occupied areas for a series of compounds with either Gd or Dy as the ion.

Gnomonic projections showed DTPA, DOTA and EDTA to have among the highest values of A_{fract} found. These chelates all have a total of nine binding atoms, including first shell waters. The gnomonic projection for these three structures and a bi-acetate compound (CSD designation VEDSEC **[10]**) are shown in Figure 7. The results are summarized in Table 3, which shows that the fractional projected area, including that from the first shell water oxygens, is between 0.629 and 0.637 for the first three compounds. Their effective projected area was exceeded by only one structure in the database, VEDSEC **[10]**, with a value of 0.670. This compound contains two acetate molecules with their carboxyl groups in a bidentate conformation and a ring structure with 6 nitrogens, for a total of ten binding atoms surrounding the Gd (Figure 7d). As indicated in the diagram **[10]**, the carboxyl groups sit above and below the plane formed by the macrocycle, and the Gd ion sits in the center. Note that the large ring is not planar, but is slightly cupped in an asymmetric fashion. It is difficult to attain higher fractional projected areas because steric effects become significant as more atoms are positioned at proper metal-ligand distances for Gd binding.

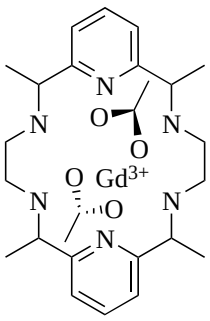

VEDSEC **[10]**

To better understand the effective area concept, it is instructive to examine some other compounds with similar or different projected areas (Table 3). Since the fractional projected area for common chelators is close to 0.63, full binding for Gd, with 9 coordination atoms, implies an effective surface area of about 0.07 surface units per atom. Table 3 shows that the fractional projected areas for Gd-chelates can range from 0.604 to 0.670. This range is about equivalent to the area occupied by one water molecule. Compound JOZGUA **[11]** has a fractional projected area that is comparable to EDTA. For that compound, the Gd ion is bound to 4 monodentate oxygens from two molecules with pyridine rings. These oxygens, combined with 2 ring nitrogens and 3 water molecules, result in a coordination of 9 and a fractional projected area of 0.630. This structure is similar to EDTA, which also contains 4 monodentate carboxylate oxygens, 2 nitrogens, and 3 water molecules. For NAOAGD **[12]**, the Gd ion is surrounded by 6 monodentate oxygens and 3 ether oxygens in 3 separate linear chain molecules. There are no waters or amide nitrogens in this structure. The ether oxygens, however, are located slightly further from the Gd ion than are carboxylate oxygens. The resulting fractional surface area is 0.625, which is somewhat lower than the value for EDTA, reflecting the larger average Gd-O distances.

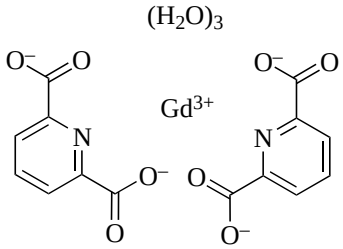

JOZGUA **[11]**

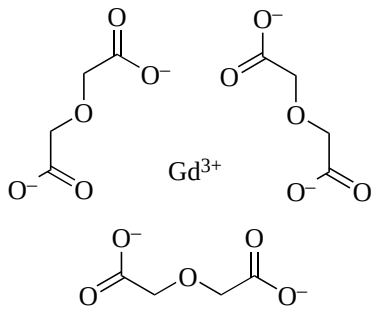

NAOAGD **[12]**

From our molecular dynamics simulations, we saw that the atoms of the first shell around the Gd ion moved in a correlated fashion. It is significant to note that when a water molecule or a chelating atom begins to move away from the Gd ion, other atoms and water molecules will move towards the metal ion so that a constant average distance for all first shell atoms, relative to the Gd ion, is maintained. Water molecules venture furthest away from the Gd ion – to a distance of 3.2 Å, relative to their normal X-ray distance of 2.4 Å. In general, any atomic movement that attempts to change the coordination number of Gd will be offset by the correlated

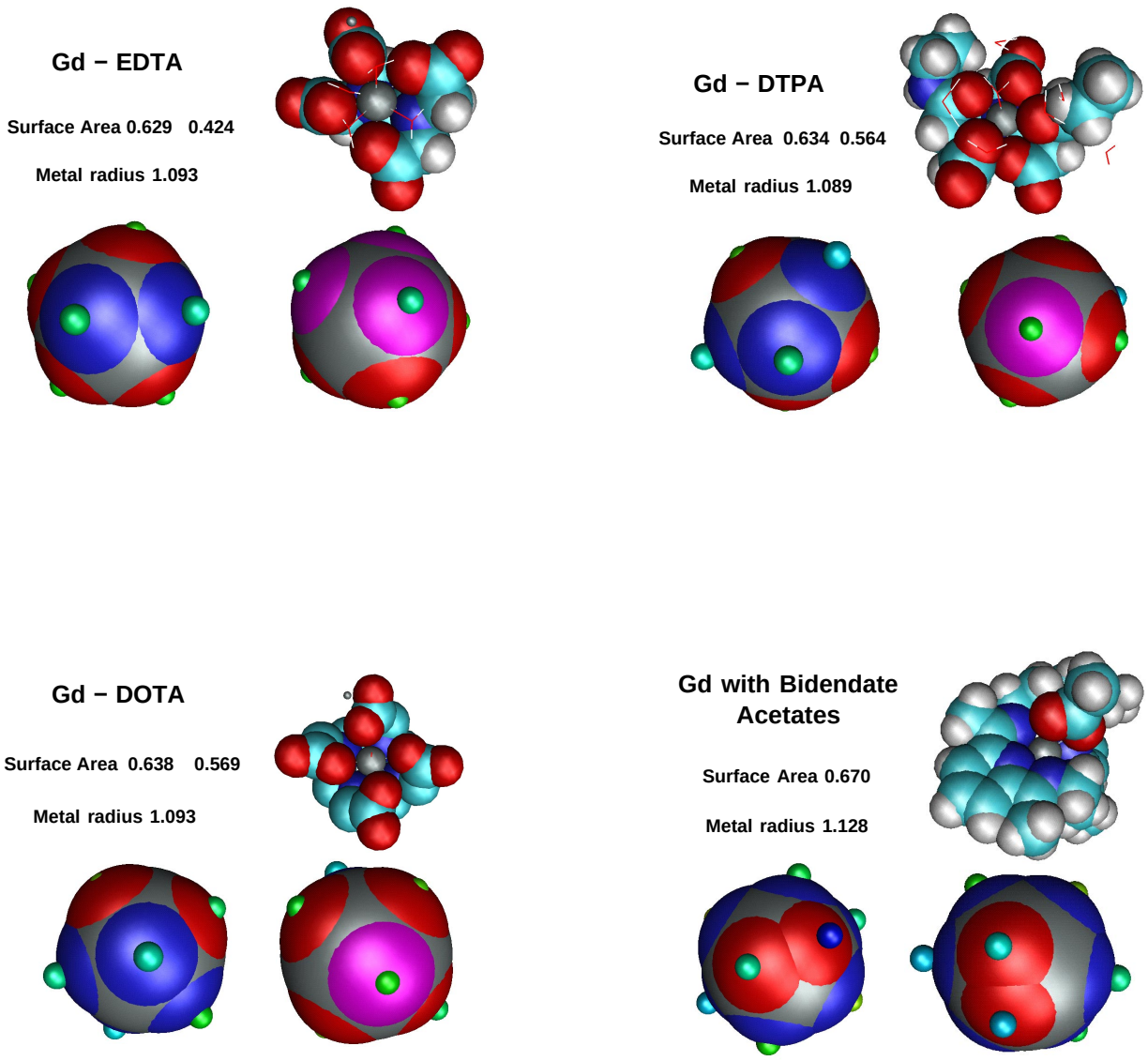

Figure 7. *Examples of gnomonic projections for 4 structures:*
(a) Gd - EDTA
(b) Gd - DTPA
(c) Gd - DOTA
(d) Gd - Bi-acetate (VEDSEC).
A model of the chelate molecule, with the Gd ion at the center, is shown in the upper right portion of each figure. The lower half of each figure shows two views of the gnomonic projection onto a gray sphere. Intersected areas for the carboxylate oxygen atoms are represented in red, water oxygens in pink, and those for the nitrogen atoms appear in blue.

motion of other atoms near the Gd ion. We can predict that chelating atoms or water molecules in other compounds will also adjust their position to maintain a coordination number of 9 for Gd.

The one X-ray structure, VEDSEC **[10]**, that shows a coordination of 10 about a Gd has no water molecules and two bidentate carboxylate groups. VEDSEC **[10]** is able to fit 10 ligand atoms around the metal because a bidentate carboxylate group takes up less space than the corresponding pair of water molecules. (See Figure 7d.) Note that the 10th ligand atom only adds a factor of 0.035 to A_{fract}, which is about half that contributed by typical ligand atoms. The static reasons for this are that the carboxyl oxygens are allowed to draw close to one another because of their chemical binding, and that both oxygens lie slightly further from the metal than do other

ligand atoms. It is interesting to compare the footprints of waters in Figs. 7 a-c (pink circles), which tend to stay away from other circles, with those for the bidentate carboxyl ligand (paired red circles) in Figure 7d. Waters have a large footprint because they lie close to the metal, and because of their high mobility relative to the other chelating groups. Figure 7d clearly shows that the carboxyl circles are smaller than those for the water oxygens, because the carboxyls are further from the metal, and that the 2 bidentate carboxyl oxygens lie close together. This results agree with the predictions from our dynamics simulations.

A case at the opposite extreme is that of structure SERYOD **[13]**. The molecular structure for SERYOD is $(H2O)_3(CF_3CO_2)GdÐ(CF_3CO_2)_4ÐGd(CF_3CO_2)(H2O)_3$ in which four carboxyl groups bind symmetrically to each of the two Gd atoms, forming a barrel. Capping each end are three waters, with their oxygens pointing at the Gd, and one more carboxyl group. One of the carboxylate oxygens in the terminal CF_3CO_2 group is shared with a Gd in the next unit cell and cannot be positioned at or near the normal binding distance of 2.4 Å. Instead it is located at 3.4 Å from the metal ion, so that SERYOD's coordination may be considered as either 8 or 9. Counting the out-of-position oxygen as a binding atom, the resulting projected area is 0.604, with a coordination of 9. If the out-of-position oxygen is excluded, the coordination number becomes 8 and the effective area is 0.571. As in VEDSEC **[10]**, the asymmetrically placed outer carboxyl group contributes only about half of the expected fractional projected area of 0.07 for a tightly binding ligand atom, principally because it cannot get in close to the Gd. These bidentate carboxylate groups increase the projected area but bind in an asymmetric, possibly metastable conformation. This is similar to the case of P3A **[5]** considered in the previous section. There, the outer carboxyl atom was by far the most mobile ligand atom seen in the dynamics simulations.

From these results, it appears that for structures with a composition similar to those of existing MRI compounds, consisting of binding carboxylate oxygens, nitrogens and water molecules, a chelate with significantly larger effective projected area will be difficult to design. There were no structures in the CSD containing at least one inner shell water that made more effective use of the area around the Gd than the known MRI compounds.

Summary

We have shown that it is possible to use molecular dynamics and mechanics simulations to evaluate the static and dynamic properties of novel chelate structures. By use of these tools, it is now possible to predict *q*-values and binding conformations for new chelate structures and evaluate their potential usefulness as MRI contrast agents. Additionally, we can calculate the magnetic resonance relaxivity for typical metal-chelate complexes.

A number of MRI chelating agents have been examined using molecular dynamics techniques. It is shown that, as expected, carboxyl groups typically assume the monodentate position in which one oxygen binds to the Gd ion (*R*(O-Gd) ~ 2.4 Å) and exhibits small rms motion. The other oxygen is further away and exhibits greater motion. The near oxygen is practically stationary while the far oxygen rotates on a lever arms whose pivot is the inner oxygen. We have also seen that motions of the chelating atoms are correlated, meaning that as one atom moves away from the metal ion, others will move closer, so that the average metal-chelate distance remains constant. These motions are a low frequency vibrational mode of the complex. The accuracy of our MD simulations in predicting *q*-values and carboxylate binding distances for reference chelates has been shown. The use of gnomonic projections provides a semi-quantitative method of evaluating how effectively binding atoms use the space surrounding the paramagnetic ion. As chelate structures, DTPA and DOTA are shown to use the space around the Gd ion most efficiently, with a fractional occupied area of about 0.64, relative to a maximum value found in the CSD of about 0.67. For other proposed structures to bind as efficiently as DTPA to the Gd ion, they will need to have comparable fractional areas, and should at the same time allow sufficient space for at least one water molecule to occupy the inner shell of the Gd ion.

Thus we have demonstrated several methods that can be used to evaluate the effectiveness of potential MRI contrast agents. Flexibility in the molecular backbone and carboxylate arms is important to make effective use of the free space around the Gd ion. This has also been discussed by Hancock.[9-11] For efficient binding to the Gd ion, with its coordination number of 9, the sum of binding carboxyl and amine groups should be 8 or more. An outstanding question is the binding strength of carboxyl groups relative to amine groups. For instance, if a structure had more amine groups than carboxyl groups, would the binding be sufficiently strong? This question needs to be addressed before we can make definitive choices between a set of candidate structures such as those analyzed here.

Several common chelating agents, like DTPA and DOTA, which are currently in clinical use, have *q*-values of 1. In this paper, molecular simulation methods have been used to predict *q*-values for proposed structures that vary from 0 to 3. It would be interesting to synthesize and test some of these molecules and examine the relationship between the predicted binding group mobility and *q*-value, the stability constant, and relaxivity.

Acknowledgments: Many helpful discussions with Dr. Kenneth Kellar, including his assistance with the magnetic relaxivity data, and the assistance of Dr. L. Castonguay in obtaining the CSD structures are gratefully acknowledged. This work was supported by the Department of Energy under contract DE-ACO4-94AL85000 and by a grant from Sterling-Winthrop, Inc.

References

1. Lauffer, R. B. *Chem.Rev.* **1987**, *87*, 901-927.
2. Koenig, S. H. and Brown, R. D. in *Magnetic Resonance Annual 1987*, H. Y. Kressel, Ed., Raven Press, New York, 1987 .
3. Koenig, S. H., Baglin, C., Brown, R. D., and Brewer, C. F. *Magn.Reson.Med.* **1984**, *1*, 496.
4. Koenig, S. H. *Israel J. Chem.* **1988**, *28*, 345.
5. Anderegg, G. in *Critical Evaluation of Equilibrium Constants in Solution*. Vol. 14 Pergamon Press, New York, 1977, 1.
6. Abragam, A., *The Principles of Nuclear Magnetism*, Clarendon Press, Oxford, 1961.
7. Hertz, H. G. in *Water: A Comprehensive Treatise.* Vol. 3, F. Franks, Ed., Plenum Press, New York, 1973, 301-399.
8. Hancock, R. D. *Pure and Applied Chem.* **1986**, *58*, 1445-1452.
9. Hancock, R. D. and Martell, A. E. *Chem.Rev.* **1989**, *89*, 1875-1914.
10. Hancock, R. D. *Acc.Chem.Res.* **1990**, *23*, 253.
11. Fossheim, R. and Dahl, S. G. *Acta Chemica Scand.* **1990**, *44*, 698-706.
12. Fossheim, R., Dugstad, H., and Dahl, S. G. *J.Med.Chem.* **1991**, *34*, 819-826.
13. Kumar, K. and Tweedle, M. F. *Inorg.Chem.* **1993**, *32*, 4193-4199.
14. Frey, S. T., Chang, C. A., Carvalho, J. F., Varadarajan, A., Schultze, L. M., Pounds, K. L., and Jr., W. d. H. *Inorg.Chem.* **1994**, *33*, 2882-2889.
15. Hay, B. *Inorg.Chem.* **1991**, *30*, 2876-2884.
16. Hay, B. *Coordination Chem. Revs.* **1993**, *126*, 177-236.
17. Rappe, A. K., Colwell, K. S., and Casewit, C. J. *Inorg. Chem.* **1993**, *32*, 3438-3450.
18. Badertscher, M., Musso, S., Welti, M., Pretsch, E., Maruizumi, T., and Ha, T.-K. *J. Comput. Chem.* **1990**, *11*, 819-828.
19. Geraldes, C. G. G. C., Brown, R. D., Brucher, E., Koenig, S. H., Sherry, A. D., and Spiller, M. *Mag. Reson. in Med.* **1992**, *27*, 284.
20. Kim, S. H., Pohost, G. M., and Elgavish, G. A. *Bioconjugate Chem.* **1992**, *3*, 20.
21. Ladd, M. F. C., Povey, D. C., and Stace, B. C. *J.Cryst.Mol.Struct.* **1974**, *4*, 313.
22. Kullnig, R. K., (Private Communication), (1993).
23. Ladd, M. F. C., Povey, D. C., and Stace, B. C. *Acta Cryst.* **1973**, *B29*, 2973.
24. Contrait, P. M. *Acta Cryst.* **1972**, *B28*, 781.
25. Shkol'nikova, L. M., Polyanchuk, G. V., Dyatlova, N. M., and Polyakova, I. A. *Zh. Strukt. Khimii.* **1984**, *25*, 103.
26. Sherry, A. D. *J.Less Common Metals* **1989**, *149*, 133.
27. Sherry, A. D., Brown, R. D., Geraldes, C. F. G. C., Koenig, S. H., Kuan, K.-T., and Spiller, M. *Inorg. Chem.* **1989**, *28*, 620.
28. Cacheris, W. P., Nickle, S. K., and Sherry, A. D. *Inorg. Chem.* **1987**, *26*, 958.
29. Berendsen, H. J. C., Grigera, J. R., and Straatsma, T. P. *J.Phys.Chem.* **1987**, *91*, 6269-6271.
30. Miyamoto, S. and Kollman, P. A. *J.Comp.Chem.* **1992**, *13*, 952-962.
31. Leach, A. R. in *Reviews in Computational Chemistry*. Vol. 2, K. B. Lipkowitz and D. B. Boyd, Ed., VCH Publishers, New York, 1991, 1-55.
32. Levitt, M. *Chemica Scripta* **1989**, *29A*, 197.
33. Levitt, M., Hirshberg, M., Sharon, R., and Daggett, V. *Comp.Phys.Comm.* **1995**, *(submitted)*,
34. Judson, R. S., Barsky, D., Faulkner, T., McGarrah, D. B., Meliu, C. F., Meza, J. C., Mori, E., Plantenga, T., and Windemuth, A., Sandia National Laboratories, 1995-SAND 95-8258. *CCEMD - Center for Computational Engineering Molecular Dynamics, Theory and Users' Guide, Version 2.2.* .
35. Windemuth, A. and Schulten, K. *Mol.Sim.* **1991**, *5*, 353-361.
36. Brooks, B. R., Bruccoleri, R. E., Olafson, B. D., States, D. J., Swaminathan, S., and Karplus, M. *J. Comput. Chem.* **1983**, *4*, 187-217.
37. QUANTA/CHARMM, Molecular Simulations, Inc., Waltham MA, 1993.
38. Colvin, M. C. and Melius, C. F., Sandia National Laboratories, 1993-SAND93-8239. *Continuum Solvent Models for Computational Chemistry*.
39. Gaussian 92, Revision A, Frisch, M. J., Trucks, G. W., Head-Gordon, M., Gill, P. M. W., Wong, M. W., Foresman, J. B., Johnson, B. G., Schlegel, H. B., Robb, M. A., Replogle, E. S., Gomperts, R., Andres, J. L., Raghavachari, K., Binkley, J. S., Gonzalez, C., Martin, R. L., Fox, D. J., Defrees, D. J., Baker, J., Stewert, J. J. P., and Pople, J. A., Gaussian, Inc., Pittsburgh PS, 1992.
40. Bertini, I. and Luchinat, C., *NMR of Paramagnetic Molecules in Biological Systems*, Benjamin/Cummings, Menlo Park, CA, 1986.
41. Hwang, L.-P. and Freed, J. *J.Chem.Phys.* **1975**, *63*, 4017-4026.
42. Kowalewski, J., Nordenskiold, L., Benetis, N., and Westlund, P.-O. *Prog.NMR Spec.* **1985**, *17*, 141-185.
43. Rubinstein, M., Baram, A., and Luz, Z. *Mol.Phys.* **1971**, *20*, 67-80.
44. Bloembergen, N., Purcell, E. M., and Pound, R. V. *Phys.Rev.* **1948**, *73*, 679.
45. Bloembergen, N. and Morgan, L. O. *J.Chem.Phys.* **1961**, *34*, 842.
46. Koenig, S. H. and Epstein, M. *J.Chem.Phys.* **1975**, *63*, 2279-2284.
47. Marcus, Y. *J.Sol.Chem.* **1983**, *12*, 271.
48. Marcus, Y. *Chem.Rev.* **1988**, *88*, 1475.